PCCP

The Stability, Electronic Structure, and Optical Absorption of Boron-nitride Diamondoids from First-principles Calculations

Journal:	*Physical Chemistry Chemical Physics*
Manuscript ID	CP-ART-04-2018-002377.R1
Article Type:	Paper
Date Submitted by the Author:	12-Jun-2018
Complete List of Authors:	Gao, Weiwei; University of Texas at Austin, The institute for computational engineering and science Hung, Linda; Toyota Research Institute Ogut, Serdar; University of Illinois at chicago Chelikowsky, James; University of Texas, Institute for Computational Engineering and Sciences

Journal Name

ARTICLE TYPE

Cite this: DOI: 10.1039/xxxxxxxxxx

The Stability, Electronic Structure, and Optical Absorption of Boron-nitride Diamondoids from First-principles Calculations†

Weiwei Gao,[a] Linda Hung,[b] Serdar Ogut,[c] and James R. Chelikowsky[a]

Received Date
Accepted Date

DOI: 10.1039/xxxxxxxxxx

www.rsc.org/journalname

Although diamondoids are broadly studied for their fundamental properties and applications, the boron-nitride-based diamondoids are scarcely explored. Here we predict the stability, electronic structure, and optical absorption spectra of six boron-nitride (BN) diamondoids with first-principles methods based on pseudopotential density functional theory and many-body perturbation methods implemented with real-space formalism. We find four of them are thermodynamically stable at room temperature, while $B_{10}N_8H_{24}$ and $B_6N_4H_{16}$ show thermodynamic instability in molecular dynamics simulations. With the GW approximation, we predicted the ionization energies and electron affinities of BN-diamondoids and find the evolution of the electronic structure with size does not follow the same trend as diamondoids, owing to the unbalanced numbers of boron and nitrogen atoms. We show strong photoabsorption of BN-triamantane and BN-adamantane in the infrared and visible range and analyze the features of low-energy absorption by examining the characteristics of related orbitals.

1 Introduction

Carbon is the fourth most abundant element of the universe and forms diverse types of materials with unusual and technologically important properties. As the nearest neighbors of carbon on the periodic table, boron and nitrogen together constitute many materials that are isoelectronic and structurally akin to carbon-based materials. Some well-studied examples include cubic boron nitride, boron nitride nanotubes[1], and borazine, which resemble diamond, carbon nanotubes, and benzene in structures, respectively.

Diamondoids are hydrocarbons where carbon atoms are bonded as diamond-like cages and hydrogen atoms passivate the surfaces of carbon cages. Diamondoids and their derivatives (such as functionalized diamondoids) are of interest owing to their potential applications in bio-technologies[2], florescent devices[3], and electron emitters[4]. The simple structures, high thermal stability, and the experimental techniques for isolating diamondoids with the desired shape and size make them ideal model systems[5] for studying nanoparticles. Because of the similarity between bulk diamond and cubic boron nitride, it is reasonable to expect the existence of stable BN-diamondoids (BN = boron nitride), which have the same diamond-like cages but with carbon replaced by boron and nitrogen. In fact, cyclotriborazane $B_3N_3H_{12}$ is a stable ring-shaped molecule which can be regarded as a segment of the diamond-like cage[6]. However, the boron nitride analogs of adamantane and higher diamondoids have not been discovered in nature or synthesized experimentally. Although BN-diamondoids have been proposed and theoretically studied[7], the thermodynamic stability and excited-state properties of BN-diamondoids remain to be thoroughly understood with more advanced first-principles methods and confirmed by experiments.

Here we present a comprehensive study on the stability, electronic structure, and optical properties of several lower boron-nitride diamondoids, including BN-adamantane, BN-diamantane, BN-triamantane, and BN-[121]tetramantane, using the state-of-art first-principles methods based on pseudopotential density functional theory, the GW approximation, and Bethe-Salpeter equation (BSE). Our study predicts the evolution of electronic structures and optical properties of BN-diamondoids with size and contrasts the differences between them and carbon-based diamondoids.

2 Computational methods

The ground-state properties of BN-diamondoids are calculated with first-principles computational methods based on density functional theory (DFT) and ab-initio pseudopotentials. DFT calculations are carried out with PARSEC[8], which solves Kohn-Sham equations by expressing related functions, e.g. potential and

[a] 201 East 24th Street, Austin, TX, USA 78712. E-mail: weiwei@ices.utexas.edu, jrc@utexas.edu
[b] 845 W. Taylor St. M/C 273, Chicago, IL 60607. E-mail: ogut@uic.edu
[c] 4440 El Camino Real, Los Altos, CA 94022. E-mail: linda.hung@tri.global

wave functions, in real space. As implemented in PARSEC, we use a spherical boundary with radius R to model confined systems and set wave functions beyond the boundary to be zero. For structural relaxation, we use a small grid spacing of 0.2 Bohr in order to converge forces and total energies. R is set to 20 a.u. for BN-adamantane, 24 a.u. for BN-diamantane and BN-triamantane, and 27 a.u. for BN-tetramantane. For calculations of excited-state properties using GW approximation and Bethe-Salpeter equation, a larger grid spacing of 0.3 Bohr and smaller R are used to ensures both affordable computational costs and converged results. Ion potentials are treated with norm-conserving pseudopotentials[9] with the Kleinman-Bylander separable form[10] and the exchange-correlation effects are described using the Perdew-Burke-Ernzerhof functional[11]. We optimize the structures of all molecules so that the residual force on each atom is less than 5×10^{-3} Ry/Bohr.

The ionization energies and electron affinities of BN-diamondoids are predicted with the GW approximation implemented in the NanoGW package[12]. Specifically, we use the full-frequency "one-shot" GW approximation, where the Green's function $G(\mathbf{r},\mathbf{r}';\omega)$ is constructed with Kohn-Sham states but not updated, and the frequency dependence of dielectric screening effects are treated explicitly, i.e., without plasmon-pole approximations. Optical absorption cross-sections are calculated by solving the Bethe-Salpeter equations[12,13].

We briefly review the formulation of the GW approximation implemented in the NanoGW package. Our GW calculations of quasiparticle energy are carried out in two steps. In the first step, we construct the polarizability operator $\Pi(\mathbf{r},\mathbf{r}';E)$, which describes the electronic screening effects. The polarizability operator is given by a summation over eigenmodes[12]:

$$\Pi(\mathbf{r},\mathbf{r}';E)=2\sum_s \rho_s(\mathbf{r})\rho_s(\mathbf{r}')\left[\frac{1}{E-\omega_s+i0^+}-\frac{1}{E+\omega_s-i0^+}\right] \quad (1)$$

where 0^+ is a positive infinitesimal number and the amplitude $\rho_s(\mathbf{r})$ is

$$\rho_s(\mathbf{r})=\sum_v^{\text{occ}}\sum_c^{\text{empty}} X_{vc}^s\phi_v(\mathbf{r})\phi_c(\mathbf{r})\left(\frac{\varepsilon_c-\varepsilon_v}{\omega_s}\right)^{1/2} \quad (2)$$

where $\phi_n(\mathbf{r})$ and ε_n are Kohn-Sham states and energy, respectively. And $\{\omega_s, X_{vc}^s\}$ in Eq. 2 and 1 are the eigenpairs of eigenvalue problem defined by the Casida's equation[14,15]

$$R^{1/2}[R+4K^x]R^{1/2}X=\omega_s^2X \quad (3)$$

The matrix elements of R and K^x are

$$R_{vc,v'c'}=\delta_{vv'}\delta_{cc'}(\varepsilon_c-\varepsilon_v)$$

$$K^x_{vc,v'c'}=\int\phi_v(\mathbf{r})\phi_c(\mathbf{r})\tfrac{1}{|\mathbf{r}-\mathbf{r}'|}\phi_{v'}(\mathbf{r}')\phi_{c'}(\mathbf{r}')d\mathbf{r}d\mathbf{r}' \quad (4)$$

With the polarizability $\Pi(\mathbf{r},\mathbf{r}';E)$, we proceed to evaluate the matrix element of self-energy operator with the GW approximation

$$\langle j|\Sigma(E')|j'\rangle=\langle j|\frac{i}{2\pi}\int e^{-iE0^+}G(E'-E)(V+V\Pi(E)V)dE|j'\rangle$$

$$=-\sum_v^{\text{occup}}K^x_{vjvj'}+2\sum_n^{\text{all states}}\sum_s\frac{V^s_{nj}V^s_{nj'}}{E-\varepsilon_n-\text{sgn}(\varepsilon_n-\mu)\omega_s} \quad (5)$$

where $V^s_{nj}=\sum_{vc}K^x_{njvc}(\frac{\varepsilon_c-\varepsilon_v}{\omega_s})^{1/2}X^s_{vc}$. In the one-shot GW approximation, the quasiparticle energy of state j is given by

$$E_j^{GW}=E_j^{KS}+\langle j|\Sigma(E_j^{GW})-V_{xc}|j\rangle \quad (6)$$

where $\Sigma(\omega)$ should be evaluated at $\omega=E_j^{GW}$. Since Eq. 6 is a non-linear equation, we solve it with the Newton-Raphson method. There are two major cutoff parameters which should be carefully converged in our calculations. The first is the radius R of the spherical boundary. The importance of converging the GW calculation with R were discussed in previous work[16,17]. The other important cutoff parameter is the number of states included in the GW calculations, which has also been discussed extensively in literature[16,18]. In principle, one should include an infinite number of unoccupied states to solve the Casida's equation (Eq. 3) and evaluate the summation in Eq. 6. However, for practical calculations, we truncate both the matrices in the Casida's equation and the summation over states by including a finite number of states. Here we denote the number of states included in a GW calculation N, and the energy corresponding to the highest state E_N. To speed up the convergence of $\langle j|\Sigma|j'\rangle$ with respect to N, we use the static-remainder approach[12,19].

3 Results and Discussion

3.1 Structures and Stability

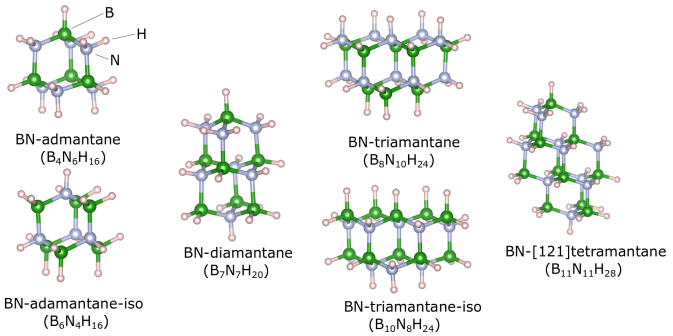

Fig. 1 Illustrations of molecular structures of BN-diamondoids.

Size and shape are the main factors affecting the electronic and optical properties of nanosized carbon materials. But for BN-diamondoids, stoichiometry is also important, i.e., the difference between the number of boron atoms and nitrogen atoms also affects their properties. For example, there are same numbers of boron and nitrogen atoms in BN-diamantane and BN-tetramantane, and they are isoelectronic to the corresponding diamondoids. However, the number of boron atoms and nitrogen atoms are different by two in both BN-triamantane and BN-adamantane. Therefore BN-triamantane and BN-adamantane are

Table 1 Comparison between the calculated atomization energies E^{at} of diamondoids and BN-diamondoids. For reference, the experimental atomization energy of adamantane is shown in the bracket.

Diamondoid	E^{at} (kcal/mol)	BN-diamondoid	E^{at} (kcal/mol)
$C_{10}H_{16}$	2713.1 (2688.05 [20])	$B_6N_4H_{16}$	2246.9
		$B_4N_6H_{16}$	2267.3
$C_{14}H_{20}$	3654.7	$B_7N_7H_{20}$	3157.0
$C_{18}H_{24}$	4594.3	$B_{10}N_8H_{24}$	3882.9
		$B_8N_{10}H_{24}$	3909.8
$C_{22}H_{28}$	5542.5	$B_{11}N_{11}H_{28}$	4763.5

not isoelectronic to their carbon-based counterparts. For convenience, we call $B_4N_6H_{16}$ as BN-adamantane, which contains two more nitrogen atoms than boron atoms, and $B_6N_4H_{16}$ BN-adamantane-iso. A similar naming convention also applies to BN-triamantane (i.e. $B_8N_{10}H_{24}$) and BN-triamantane-iso (i.e. $B_{10}N_8H_{24}$).

The relaxed structures of BN-diamondoids are similar to those of diamondoids, as shown in Figure 1. Nevertheless, close examinations of their structures reveal small distortions of boron and nitrogen atoms. These distortions lower the symmetry of BN-diamondoids. The boron-nitrogen bond lengths of BN-diamondoids range from 1.49 to 1.66 angstrom with an average of 1.55 angstrom, slightly smaller than that of cubic boron nitride. For reference, we provided the structural models of six BN-diamondoids in the supplementary material.

As a measure of the strength of bonds, we compute the atomization energy of BN-diamondoids defined as

$$E^{at}(B_nN_mH_s) = nE^{tot}(B) + mE^{tot}(N) + sE^{tot}(H) - E^{tot}(B_nN_mH_s) \quad (7)$$

where E^{at} denotes atomization energy and E^{tot} denotes total energy. The calculated atomization energy of adamantane agrees well with the experimental value[20], as shown in Table 1. In general, we find the atomization energy E^{at} of BN-diamondoids is smaller than corresponding diamondoids by about 8 percent, suggesting BN-diamondoids are less stable than diamondoids. To crosscheck our results, we also conducted the same calculations of atomization energies with the plane-wave based code Quantum Espresso[21,22] and obtain the same conclusion. This observation is different from previous work[7], which uses relative total energy to compare the stability of diamondoids and corresponding BN-diamondoids. Our work, however, uses the atomization energy to gauge the strength of the chemical bonds in these systems. Moreover, by comparing the atomization energies, we infer BN-adamantane (BN-triamantane) is more stable than BN-adamantane-iso (BN-triamantane-iso).

For further assessments of the thermodynamic stability of BN-diamondoids, we perform molecular dynamics (MD) simulations for all six BN-diamondoids. All the systems are modeled in a canonical ensemble. The temperature is controlled around 300 K with the Langevin thermostat and the time step is set to a small value 10 a.u. (≈ 0.242 fs) in order to account for the fast motion of hydrogen atoms. The friction coefficient for Langevin dynamics is set to 10^{-4} a.u and a small grid spacing 0.2 Bohr is used for converged calculations of forces. Both BN-adamantane-iso and BN-triamantane-iso demonstrate structural instability by showing that hydrogen atoms are detached from some boron atoms within 1 ps. The other four molecules studied in this work do not show structural instability in our MD simulations. These findings also support that BN-adamantane-iso (BN-triamantane-iso) is less stable than BN-adamantane (BN-triamantane).

3.2 Electronic Structure and Optical Absorption Spectra

From the DFT-PBE calculations, we find interesting differences between the electronic structure of BN-diamondoids and diamondoids. For example, although most BN-diamondoids we investigated here have a non-magnetic ground state, BN-admantane-iso $B_6N_4H_{16}$ and BN-triamantane-iso $B_{10}N_8H_{24}$ have spin-polarization of $2\mu_B$ (2 Bohr magneton) at ground state. The small HOMO-LUMO gap of ~ 0.2 eV given by DFT calculations also indicates the high chemical reactivity of them. Moreover, we find there is a singlet ground-state with similar total energy if we manually constrain the total spin to zero and relax the system.

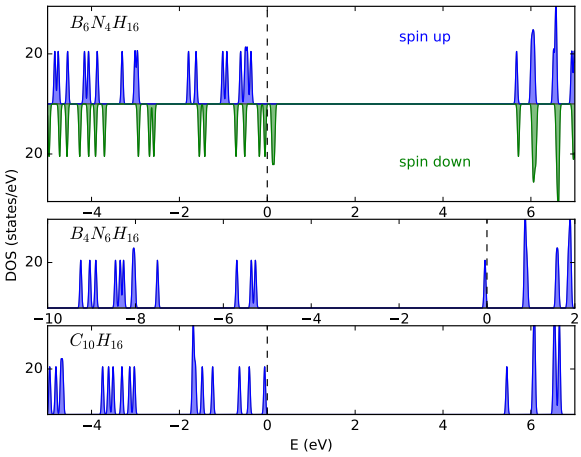

Fig. 2 Comparison between the electron density of states (DOS) of BN-adamantane-iso, BN-adamantane, and adamantane. The energy of highest occupied state is set to zero. The degeneracy of some states is lifted owing to the low-symmetry relaxed structure used here.

The 'unusual' spin polarization can be explained qualitatively by comparing the DOS of BN-diamondoids with diamondoids and considering the shell model of superatoms or nanocrystals. If we consider carbon-based adamantane as a close-shell superatom, then BN-adamantane-iso lacks 2 electrons from close-shell electron configuration. Therefore, it should have a 2 Bohr magneton ground state according to the Hund's rule, and the exchange splitting is ~ 0.5 eV, as shown in the top panel of Figure 2. On the other hand, BN-adamantane has two more electrons than the close-shell configuration. Since two extra electrons happen to fill an s-like subshell, BN-adamantane doesn't have spin polarizations at the ground state. This is also reflected in the DOS of BN-adamantane $B_4N_6H_{10}$, as shown in the middle panel of Figure 2, where we recognize the states of BN-adamantane below -5.0 eV as the filled electron shell that are

qualitatively similar to the occupied states of admantane, and the HOMO as the s-like subshell. The shell model of nanocrystals also support our previous observation on atomization energies $E^{at}(B_6N_4H_{16}) < E^{at}(B_4N_6H_{16})$, since $B_4N_6H_{16}$ has a filled subshell while $B_6N_4H_{16}$ has an unfilled subshell. Similarly, the same argument also applies to BN-triamantane-iso and BN-triamantane. Moreover, BN-diamantane and BN-tetramantane are isoelectronic to their carbon-based counterparts. We consider them as close-shell systems, which obviously have no spin polarizations at the ground state. Detailed comparison between the density of states of the other four stable BN-diamondoids and the related diamondoids are provided in the supplementary material.

Full-frequency G^0W^0 calculations are conducted for the vertical ionization potentials (IP) and electron affinities (EA) of four BN-diamondoids (i.e. $B_4N_6H_{16}$, $B_7N_7H_{20}$, $B_8N_{10}H_{24}$, and $B_{11}N_{11}H_{28}$) and the corresponding diamondoids. Based on the DFT calculations, both BN-adamantane-iso and BN-triamantane-iso are highly reactive with small gaps, and MD simulations also demonstrate their thermodynamic instability. Therefore we don't consider their GW quasiparticle energies in this work.

We emphasize the cutoff parameters R and E_N should be carefully chosen to obtain converged results. The convergence speed of GW self-energy matrix elements $\langle j|\Sigma(E)|j\rangle$ with respect to R and E_N sensitively depend on the characters of orbitals $|j\rangle$. For example, Figure 3 shows how the computed electron affinity and ionization potential of BN-diamantane change with respect to convergence parameters R and E_N. As compared to EA, the IP of BN-diamantane converges faster with respect to R. We can see $R = 14$ a.u. is good enough to converge the ionization potential of BN-diamantane, while the electron affinity requires $R = 18$ a.u to converge. On the other hand, IP converges much slower with respect to E_N. Even $E_N = 80$ eV is not sufficient to ensure the convergence of ionization potential within 0.1 eV. Fully converging both EA and IP at the same time requires at least $R = 18$ a.u. and $E_N > 80$ eV, which requires significant computational resources to accomplish. Following previous work[16], we extrapolate the converged GW quasiparticle energies by fitting $E^{GW}(N)$ calculated with different number of bands N with the relation $E^{GW}(N) = E^{GW}(\infty) + \frac{c_1}{N+c_2}$, where $E^{GW}(\infty)$ is the converged energy, and c_1 and c_2 are fitting parameters.

In Table 2, we compare the calculated ionization potentials and electron affinities of BN-diamondoids with those of diamondoids. For diamondoids, we find that the calculated ionization potentials agree with experimental values very well. BN-diamondoids have smaller ionization energies compared to the corresponding diamondoids with the same number of atoms. In particular, BN-adamantane and BN-triamantane have small ionization potentials of less than 4.0 eV. The calculated electron affinities of diamondoids are all negative, which agree with previous reports[4], while all BN-diamondoids studied here have positive electron affinities. Because of the quantum confinement effects, HOMO-LUMO gaps of diamondoids decrease monotonously as the size of molecules increase. In contrast, the evolution of the electronic structure of BN-diamondoids does not follow the same trend as carbon-based diamondoids. For example, BN-admantane and BN-triamantane have smaller HOMO-LUMO gaps

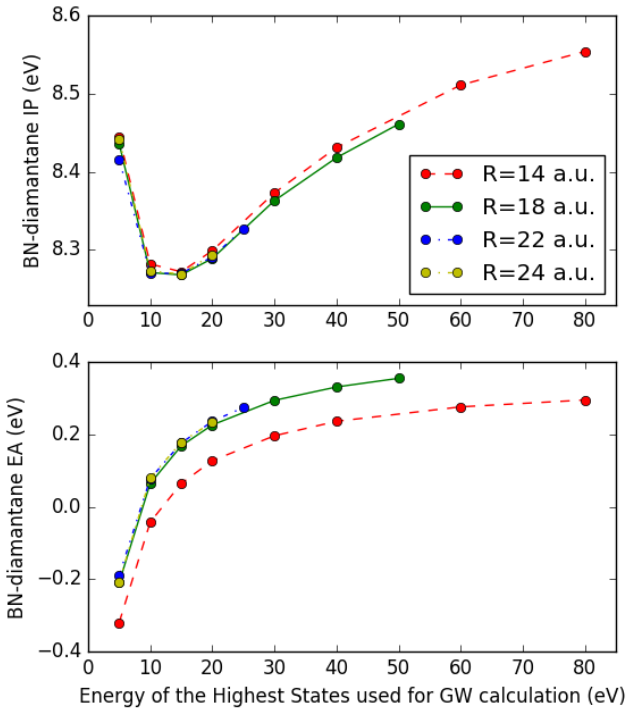

Fig. 3 Ionization potential and electron affinity of BN-diamantane calculated with different parameters are shown to illustrate the convergence of GW results. Here different curves correspond to calculations with different R, and each curve shows the change of GW quasiparticle energy with E_N.

than BN-diamantane and BN-tetramantane. In fact, we find the HOMO-LUMO gaps of BN-adamantane, BN-triamantane, and BN-[121]tetramantane are even smaller than the band gap of cubic boron nitride, 6.4 eV[23]. The small electronic gap of BN-adamantane and BN-triamantane can be simply explained by the fact that they have two extra electrons than the close-shell configuration, as we discussed previously. However, the small electronic gap of BN-[121]tetramantane is unexpected.

By solving the Bethe-Salpeter equation, we obtained the energy and wave functions of excitonic states, from which the photoabsorption spectra are calculated with a Gaussian broadening of 0.1 eV. In Figure 4, we plot the absorption spectra of four BN-diamondoids, and also marked the HOMO-LUMO gaps E_g and the lowest exciton energy E_g^{opt} (i.e., the optical gap) with arrows. As expected, the excitonic effects are strong due to the week screening in nanosized BN-diamondoids. The binding energy of the lowest exciton in BN-diamondoids have similar magnitude ($2.0 \sim 3.0$ eV) as those of carbon diamondoids[25]. The absorption cross-section spectra of four BN-diamondoids share few similarities and are highly dependent on their shapes and sizes. For BN-adamantane and BN-triamantane, the photoabsorption is strong around $E = 1.0$ eV, which suggests potential applications such as photovoltaic devices working in the infrared and visible ranges. The absorption becomes weaker when photon energy ranges from 3 eV to 6 eV. Differently, the low-energy absorption

Table 2 Ionization potential, electron affinity, and HOMO-LUMO energy gap of BN-diamondoids and diamondoids calculated with GW approximation. The experimental ionization energies of diamondoids are also presented for reference.

Molecule	IP (eV)	Expt. IP (eV)	EA (eV)	HOMO-LUMO gap (eV)
BN-admantane	3.77	–	0.78	2.99
BN-diamantane	8.69	–	0.44	8.25
BN-triamantane	3.39	–	1.03	2.36
BN-[121]tetramantane	6.92	–	1.43	5.49
Adamantane	9.48	9.23 ± 0.12 [24]	-0.59	10.07
Diamantane	9.18	8.80 ± 0.06 [24]	-0.50	9.68
triamantane	8.75	8.57 ± 0.08 [24]	-0.48	9.23
[121]tetramantane	8.62	8.23 [25]	-0.40	9.02

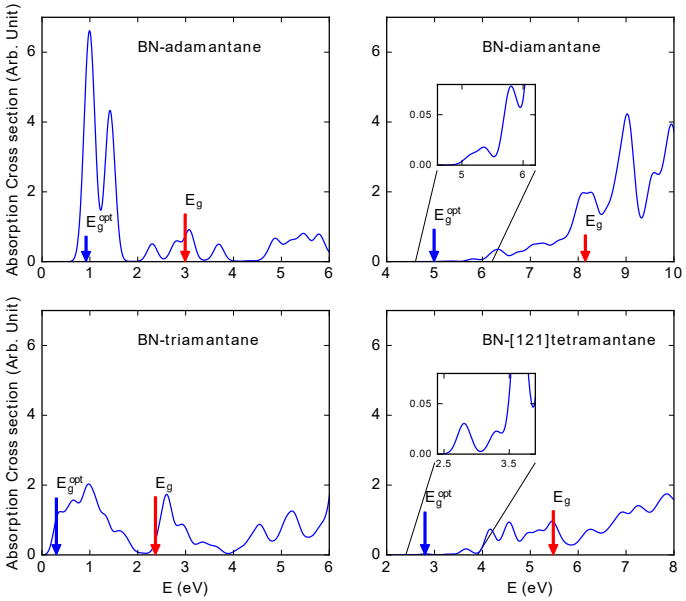

Fig. 4 Photoabsorption cross-section of BN-diamondoids calculated by solving BSE. HOMO-LUMO energy gap E_g and the lowest exciton energy E_g^{opt} are marked with red and blue arrows respectively.

of BN-diamantane and BN-tetramantane is significantly quenched and absorption cross section increases slowly as photon energy goes higher. The insets of Figure 4 show the magnified plots of the low-energy absorption cross-section spectra of BN-diamantane and BN-[121]tetramantane. For BN-[121]tetramantane, we can see the oscillator strength of the lowest excitations are smaller than excitations in $4 \sim 8$ eV range by nearly two orders of magnitude.

To understand why low-energy absorption spectra are markedly different between BN-diamondoids, we examine the characteristics of the lowest-energy excitons. As the Bethe-Salpeter equation is solved with the Tamm-Dancoff approximation [13], excitonic state $|S\rangle$ can be written as a linear combination of products of hole state $|v\rangle$ and electron state $|c\rangle$

$$|S\rangle = \sum_{cv} X_{cv}^S |c\rangle|v\rangle \tag{8}$$

where the coefficients X_{cv}^S satisfy the normalization condition $\sum_{cv} |X_{cv}^S|^2 = 1$ and tell us which single particle transition $|v\rangle \rightarrow |c\rangle$ mainly contributes to a exciton $|S\rangle$. Table 3 presents the transitions that contribute most to the lowest two excitons of each BN-diamondoid.

Table 3 Transitions that contribute most to the lowest-energy and the second lowest-energy excitonic states. H-1 stands for the states right below highest occupied molecule orbital (HOMO), and L+i means the i-th orbital higher than the lowest unoccupied molecule orbital (LUMO). The percentages in the brackets are the weights of transitions, i.e. $|X_{cv}^S|^2$, in excitonic states.

Molecule	The lowest exciton	The second lowest exciton
BN-adamantane	H $\rightarrow$ L+2 (59%) H $\rightarrow$ L+1 (12%) H $\rightarrow$ L+4 (13%)	H $\rightarrow$ L (37%) H $\rightarrow$ L+3 (31%) H $\rightarrow$ L+2 (14%)
BN-diamantane	H $\rightarrow$ L (93%)	H-1 $\rightarrow$ L (91%)
BN-triamantane	H $\rightarrow$ L (82%) H $\rightarrow$ L+4 (12%)	H $\rightarrow$ L+2 (82%) H $\rightarrow$ L+5 (11%)
BN-tetramantane	H $\rightarrow$ L (97%)	H-1 $\rightarrow$ L (94%)

For BN-[121]tetramantane, 97 percent of the lowest excitonic state consists of the transition from HOMO to LUMO and 94 percent of the second lowest excitonic state consists of the transition from HOMO-1 to LUMO, therefore we focus on these three orbitals. The projected density of state (PDOS) in Figure 5 (d) shows that both HOMO-1 and HOMO of BN-[121]tetramantane mainly has characters of nitrogen p, boron p, and hydrogen s orbitals, and LUMO mainly has the characters of nitrogen p, nitrogen s, and hydrogen s orbitals. At first sight, the transition from HOMO to LUMO seems to be dipole-allowed according to our analysis of PDOS. However, if we plot orbitals in real space, as shown in Figure 5 (d), one can easily see both HOMO-1 and HOMO are localized at the lower end of BN-tetramantane, while LUMO is more delocalized and mainly located at the opposite end of the molecule. As a consequence, the spatial overlap between HOMO and LUMO is small, and therefore the oscillator strength $|\langle c|\beta|v\rangle|^2$ (β is Cartesian coordinates x, y, or z) is suppressed, which explains the weak absorption of BN-[121]tetramantane at low-energy range. Similarly, the two lowest energy excitons of BN-diamantane are mainly composed of transitions from HOMO or HOMO-1 to LUMO, and the overlap between related orbitals are also very small, as shown in Figure 5 (b). Therefore the oscillator strength corresponding to the lowest-energy exciton of BN-diamantane are small.

On the other hand, the low-energy excitons of BN-admantane

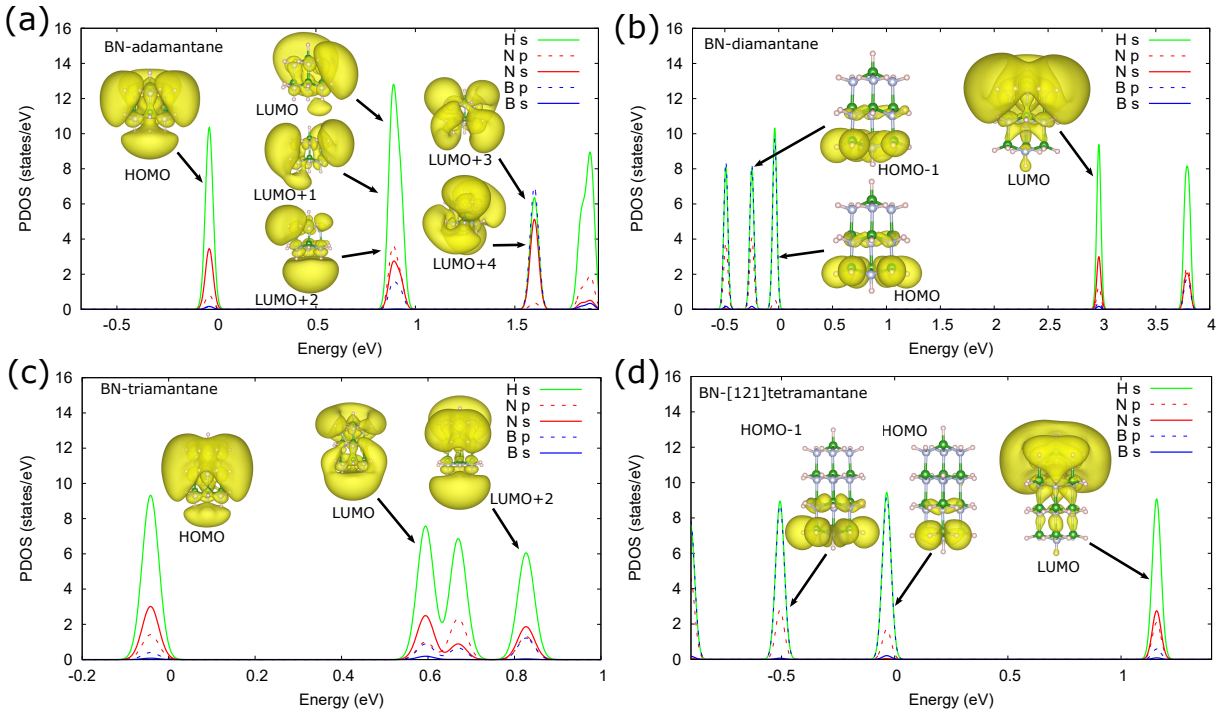

Fig. 5 Projected density of states and the illustration of molecule orbitals of (a) BN-adamantane, (b) BN-diamantane, (c) triamantane, and (d) BN-[121]tetramantane. The yellow isosurface include more than 80 percent charge density of each orbital.

and BN-triamantane are composed of transitions from HOMO to a few low-energy unoccupied states. For example, the lowest two excitonic states of BN-adamantane are mainly composed of transitions from HOMO to LUMO $\sim$ LUMO+5 (i.e., ranging from LUMO to the fifth state higher than LUMO), as shown in Table 3. Figure 5 (a) shows related orbitals in real space and demonstrates substantial spatial overlap between HOMO and the lowest five unoccupied states. Such large orbital overlaps explain the large low-energy absorption cross-section observed in BN-adamantane. And we mention the same argument also applies to BN-triamantane, as show in Figure 5 (c).

4 Conclusions

In summary, the stability, electronic structure and optical properties of BN-diamondoids are predicted with first-principles methods. Compared to diamondoids, BN-diamondoids have smaller atomization energies, demonstrating that BN-diamondoids have weaker bonds between the atoms and are less stable than diamondoids. Molecular dynamics simulations show that except for BN-adamantane-iso and BN-triamantane-iso, the other four BN-diamondoids, i.e., $B_4N_6H_{16}$, $B_7N_7H_{20}$, $B_8N_{10}H_{24}$, and $B_{11}N_{11}H_{28}$, are thermodynamically stable at room temperature. The ionization potential, electron affinity, and the HOMO-LUMO gap of BN-diamondoids are calculated with the GW approximation and compared with diamondoids. We observe that the change of gap of BN-diamondoids doesn't follow the common decreasing trend as nanoparticle size increases. In particular, the HOMO-LUMO gaps of BN-adamantane, BN-triamantane, and BN-[121]tetramantane are smaller than the band gap of cubic boron nitride. Finally, we calculate the absorption cross-section spectra of BN-diamondoids by solving the Bethe-Salpeter equation and find they are highly dependent on the size and shapes of BN-diamondoids. The low-energy absorption cross-section of BN-diamantane and BN-tetramantane is highly suppressed as compared to BN-adamantane and BN-triamantane. This observation is explained by analyzing the spatial overlaps between related electron and hole orbitals.

Conflicts of interest

There are no conflicts to declare.

Acknowledgements

W.G. and J.R.C. acknowledge support from the U.S. Department of Energy (DOE) for work on nanostructures from Grant No. DE-FG02-06ER46286, and on algorithms by a subaward from the Center for Computational Study of Excited-State Phenomena in Energy Materials at the Lawrence Berkeley National Laboratory, which is funded by the U.S. Department of Energy, Office of Science, Basic Energy Sciences, Materials Sciences and Engineering Division under Contract No. DEAC02-05CH11231, as part of the Computational Materials Sciences Program. L.H. and S.O. acknowledge support from the U.S. Department of Energy grant No. DE-SC0017824. Computational resources are provided in part by the National Energy Research Scientific Computing Center (NERSC) and the Texas Advanced Computing Center (TACC).

Notes and references

1 N. G. Chopra, R. J. Luyken, K. Cherrey, V. H. Crespi, M. L. Cohen, S. G. Louie and A. Zettl, *Science*, 1995, **269**, 966–967.
2 G. Ali Mansoori, in *Diamondoid Molecules*, John Wiley & Sons,

Inc., 2008, pp. 207–258.
3 T. Rander, T. Bischoff, A. Knecht, D. Wolter, R. Richter, A. Merli and T. MÃűller, *Journal of the American Chemical Society*, 2017, **139**, 11132–11137.
4 N. D. Drummond, A. J. Williamson, R. J. Needs and G. Galli, *Phys. Rev. Lett.*, 2005, **95**, 096801.
5 W. A. Clay, J. E. P. Dahl, R. M. K. Carlson, N. A. Melosh and Z.-X. Shen, *Reports on Progress in Physics*, 2015, **78**, 016501.
6 P. W. R. Corfield and S. G. Shore, *Journal of the American Chemical Society*, 1973, **95**, 1480–1487.
7 M. Fyta, *Nanotechnology*, 2014, **25**, 365601.
8 L. Kronik, A. Makmal, M. L. Tiago, M. M. G. Alemany, M. Jain, X. Huang, Y. Saad and J. R. Chelikowsky, *physica status solidi (b)*, 2006, **243**, 1063–1079.
9 N. Troullier and J. L. Martins, *Phys. Rev. B*, 1991, **43**, 1993–2006.
10 L. Kleinman and D. M. Bylander, *Phys. Rev. Lett.*, 1982, **48**, 1425–1428.
11 J. P. Perdew, K. Burke and M. Ernzerhof, *Phys. Rev. Lett.*, 1996, **77**, 3865–3868.
12 M. L. Tiago and J. R. Chelikowsky, *Phys. Rev. B*, 2006, **73**, 205334.
13 M. Rohlfing and S. G. Louie, *Phys. Rev. B*, 2000, **62**, 4927–4944.
14 M. E. Casida, *Recent Advances in Density Functional Methods*, World Scientific, Singapore, 1995, p. 155.
15 I. Vasiliev, S. Öğüt and J. R. Chelikowsky, *Phys. Rev. B*, 2002, **65**, 115416.
16 L. Hung, F. Bruneval, K. Baishya and S. Öğüt, *Journal of Chemical Theory and Computation*, 2017, **13**, 2135–2146.
17 L. Hung, F. H. da Jornada, J. Souto-Casares, J. R. Chelikowsky, S. G. Louie and S. Öğüt, *Phys. Rev. B*, 2016, **94**, 085125.
18 B.-C. Shih, Y. Xue, P. Zhang, M. L. Cohen and S. G. Louie, *Phys. Rev. Lett.*, 2010, **105**, 146401.
19 J. Deslippe, G. Samsonidze, M. Jain, M. L. Cohen and S. G. Louie, *Phys. Rev. B*, 2013, **87**, 165124.
20 S. Fliszar, *Atoms, Chemical Bonds and Bond Dissociation Energies*, Springer, 1994.
21 P. Giannozzi, O. Andreussi, T. Brumme, O. Bunau, M. B. Nardelli, M. Calandra, R. Car, C. Cavazzoni, D. Ceresoli, M. Cococcioni, N. Colonna, I. Carnimeo, A. D. Corso, S. de Gironcoli, P. Delugas, R. A. D. Jr, A. Ferretti, A. Floris, G. Fratesi, G. Fugallo, R. Gebauer, U. Gerstmann, F. Giustino, T. Gorni, J. Jia, M. Kawamura, H.-Y. Ko, A. Kokalj, E. Kucukbenli, M. Lazzeri, M. Marsili, N. Marzari, F. Mauri, N. L. Nguyen, H.-V. Nguyen, A. O. de-la Roza, L. Paulatto, S. Ponce, D. Rocca, R. Sabatini, B. Santra, M. Schlipf, A. P. Seitsonen, A. Smogunov, I. Timrov, T. Thonhauser, P. Umari, N. Vast, X. Wu and S. Baroni, *Journal of Physics: Condensed Matter*, 2017, **29**, 465901.
22 P. Giannozzi, S. Baroni, N. Bonini, M. Calandra, R. Car, C. Cavazzoni, D. Ceresoli, G. L. Chiarotti, M. Cococcioni, I. Dabo, A. Dal Corso, S. de Gironcoli, S. Fabris, G. Fratesi, R. Gebauer, U. Gerstmann, C. Gougoussis, A. Kokalj, M. Lazzeri, L. Martin-Samos, N. Marzari, F. Mauri, R. Mazzarello, S. Paolini, A. Pasquarello, L. Paulatto, C. Sbraccia, S. Scandolo, G. Sclauzero, A. P. Seitsonen, A. Smogunov, P. Umari and R. M. Wentzcovitch, *Journal of Physics: Condensed Matter*, 2009, **21**, 395502 (19pp).
23 D. A. Evans, A. G. McGlynn, B. M. Towlson, M. Gunn, D. Jones, T. E. Jenkins, R. Winter and N. R. J. Poolton, *Journal of Physics: Condensed Matter*, 2008, **20**, 075233.
24 K. Lenzke, L. Landt, M. Hoener, H. Thomas, J. E. Dahl, S. G. Liu, R. M. K. Carlson, T. MÃűller and C. Bostedt, *The Journal of Chemical Physics*, 2007, **127**, 084320.
25 H. Yin, Y. Ma, X. Hao, J. Mu, C. Liu and Z. Yi, *The Journal of Chemical Physics*, 2014, **140**, 214315.

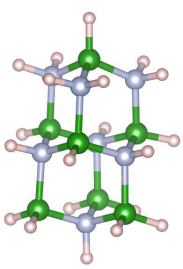

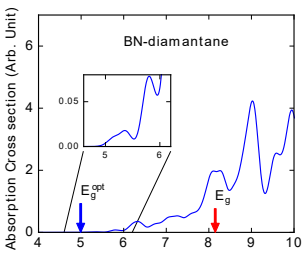
BN-diamantane
Absorption Cross section (Arb. Unit)
E_g^{opt}
E_g
0
2
4
6
4
5
6
7
8
9
10
0.00
0.05
5
6